



HAL
open science

Assessment for stretchability condition of polymers and Time-Temperature Superposition Principle; first step towards a test for recycled PET?

Noëlle Billon

► **To cite this version:**

Noëlle Billon. Assessment for stretchability condition of polymers and Time-Temperature Superposition Principle; first step towards a test for recycled PET?. *Polymer*, 2021, 231, pp.124145. 10.1016/j.polymer.2021.124145 . hal-03335032

HAL Id: hal-03335032

<https://minesparis-psl.hal.science/hal-03335032>

Submitted on 16 Oct 2023

HAL is a multi-disciplinary open access archive for the deposit and dissemination of scientific research documents, whether they are published or not. The documents may come from teaching and research institutions in France or abroad, or from public or private research centers.

L'archive ouverte pluridisciplinaire **HAL**, est destinée au dépôt et à la diffusion de documents scientifiques de niveau recherche, publiés ou non, émanant des établissements d'enseignement et de recherche français ou étrangers, des laboratoires publics ou privés.



Distributed under a Creative Commons Attribution - NonCommercial 4.0 International License

Assessment for Stretchability Condition of Polymers and Time-Temperature Superposition Principle; First Step Towards a Test for Recycled PET?

Noëlle BILLON

MINES ParisTech, Université PSL, Centre de mise en forme des matériaux (CEMEF), CNRS
UMR 7635, Sophia Antipolis, France

Corresponding author: noelle.billon@mines-paristech.fr

Abstract:

In this study the stretchability and the suitability for blow molding processes of five grades of PET are assessed within that frame of Time-Temperature Superposition Principle (TTP) where testing conditions is described with one-unique parameter: The equivalent strain-rate at reference temperature. PETs were chosen to exhibit significantly different behaviors representative for part of the variability of behavior that could exist in recycled materials. A route to anticipate stretching conditions of different resins from DMA analysis is then validated that should be extended to account for the expected variabilities in stretchability of recycled materials in an industrial context.

Keywords: bi axial stretching, stretchability, time temperature superposition principle, master curve, Polyethylene Terephthalate, ISBM, Recycling

1. Introduction

Nowadays significant efforts focus on recycling of plastic wastes. In that context, Polyethylene Terephthalate (PET) packaging, i.e., bottles, is an important challenge to be faced. Among all the possible route for recycling / reusing PET, the so-called “packaging to packaging” solution deserves to be studied.

However, PET resins that coexist on the market can combine variable types of comonomers. This results in chains of different architectures and lengths. Therefore, their forming ranges are different enough to make it necessary to adapt the processing conditions to the resin itself [1]. Unfortunately, those various polymers cannot be sort. In consequence, recycled PET will consist in blends of different resins. Without underestimating the other aspects of the problem (contaminants, quiescent crystallization, safety etc.) an essential step to be fulfilled is then to better anticipate stretchability of PET of diverse (and uncontrolled) natures and origins whereas nowadays protocols rely on the relatively low scattering of characteristics of individual neat resins. Our purpose, in this paper, is to illustrate a possible scientific route to assess stretching conditions which ensure a given extensibility to a PET and that could be extrapolated to processing of recycled materials. Question is: how to assess the respective loading conditions for two PETs, for them to develop the same extensions? For simplicity this will be named “stretchability” in the following.

In parallel (but not contradictorily) with more complete studies that use actual recycled resources, the sub-questions we intend to first answer to in simpler conditions, are: what are the measurable parameters that could enable to assess stretchability of PETs of different natures and how these parameters could they be included into procedures for material reception or for the online control of the processing? Indeed, this is two of the first and crucial demands from industry before it fully invests in recycled PET for mass production.

To achieve our aims, ISBM is considered as an example of processing application. This technic is decomposed into three steps. Firstly, a thick and amorphous preform is injection molded. Secondly, the preform is heated up to a temperature for which the material reaches its rubber like state but does not crystallize (at least during the duration of the heating up). Thirdly, the preform is simultaneously stretched and blown in a cold mold. During that blowing, a strain-induced crystallization occurs, which controls final properties of the bottle and constrains processing kinematics itself (due to the related strain hardening). The actual thermomechanical history encountered by the material is then basically biaxial and complex and can depend strongly on the processing conditions and on the stretchability of the resin.

This last step is the one we focused on in the study. More precisely, the study was conducted as follow:

- Firstly, a set of “neat” resins, potentially used in ISBM, was chosen. Laboratory characterization of those latter focused on some of the main characteristics known to be involved in

stretchability of PET [1]. In parallel, the wideness of possible behaviors of PETs for ISBM could be explored.

- Secondly, to remain close to targeted actual conditions, stretchability was assessed using an instrumented prototype for free stretch-blowing (i.e., without mold). This house made apparatus allowed in situ measurements for deformation and mechanical parameters. It was developed by the authors in the past [1-3] and exhibited a good capability to reproduce faithfully industrial stretch blow molding. Some more recent devices are described and used in the literature [4]. Prior to that step, materials were injected as preform according to state of the art, ensuring that PETs remained amorphous.

- Thirdly, correlation was made between results of “biaxial tension” at controlled temperatures and the intrinsic characteristics of the resins. Specific attention was paid to the α transition as stretching takes place above the glass transition temperature. We also suggest taking advantage of the so-called time temperature superposition principle (TTP) to assess effects of temperature and strain rate in a combined manner. Indeed, it was demonstrated in the past that this principle, which finds its origin in the analysis of linear viscoelasticity [5], could be extended to high strain [6-8]. Our analysis relied on the notion of equivalent strain rate at reference temperature successfully used for mechanical characterization of amorphous [9-12] or semi crystalline polymers [12-14] and already validated for polyesters such as PET [15, 16].

- Finally, we drew some general aspects of a possible protocol to assess, prior to blowing, stretchability of an unknown resin compared to a reference one.

This paper first presents polymers and describes biaxial tests and loading/deformation kinematics. Analysis within the frame of TTP is then developed and validated. To conclude, a protocol to characterize resins is proposed with the goal of blowing any of them in an equivalent manner (in terms of kinematics) than a reference resin. Some further developments are finally suggested.

2. Materials; Characteristics and properties of PET

The set of resins intends to be representative for some of the routes that enable designing PET chains. Different molar masses are then considered. In parallel, three types of copolymerization are used:

1. Diethylene glycol (DEG) decreases chain stiffness. It forms during the synthesis of PET and its concentration can be reduced. It slows down the crystallization kinetics.
2. Isophthalic acid (IPA) is also known to delay crystallization but increases chain stiffness.
3. Trimethylolpropane (TMP) introduces some branching.

Molecular weights of copolymers were measured using size-exclusion chromatography (SEC). However, such measurements were not possible for two of them because of dissolution problems.

PETs are characterized using their viscosity index (VI) which is an image of the viscosity of highly diluted solution and that is related to molecular weight. Consequently, in the following the polymers will be referred to through their VI, 1 to 5, from the lowest to the highest. A wide range from 0.707 to 1.03 dL/g was thus addressed. All the characteristics are gathered in Table 1.

Reference	DEG (% mol.)	IPA (% mol.)	TMP (% mol.)	VI (10mL/g)	M _n (g/mol)	M _w (g/mol)	M _z (g/mol)
VI_1	2.2	0.2	0	707	33400	55700	90200
VI_2	3.9	2.4	0.4	834	38600	78000	159000
VI_3	2.0	2.1	0	844	34400	68600	125000
VI_4	1.3	0	0	950	No dissolution		
VI_5	1.3	0	0	1030	No dissolution		

Table 1: Main characteristic of PET resins used in the study [1]

VI_3 is a “medium range” resin recommended for packaging of still water. We’ll consider it as a kind of reference in the following.

Indeed, since a long-time, molecular description has proved enlightening the understanding of deformation processes during forming (e.g., [1, 16-21] or more simply of the intrinsic stretchability of various types of materials, e.g, PEF [16], PLA [19], PVC [20], PET [21]). Despite of this, today knowledge does not allow to draw direct links between the chain architecture and the behavior of PETs. As a matter of fact, VI is often used of an input parameter but is not enough to characterize stretchability of resins.

The types of conditions we are interested in, consist in an intense stretching step of initially amorphous polymers. As far as PET-like polymers are concerned, a strain induced crystallization is observed. From a physical point of view, from previous studies (in example, [1, 22-28]) high stretchability for polymers is achieved when loading conditions (i.e., temperature, T, combined with strain rate, $\dot{\epsilon}$) ensure that polymer is loaded above its α transition, in its rubber like state. In case where polymer is initially amorphous and can exhibit strain induced crystallization, additional constrain is to avoid crystallization in static conditions and consequently making sure that temperature is lower than crystallization temperature.

The range of working temperatures were estimated using Dynamical Mechanical Analysis (DMA) for the five materials (Figure 1). Measurements were performed using a Tritec 2000 DAM, Bohlin Instruments apparatus, operated in the single cantilever deformation mode, with an imposed displacement of 5 μm to remain in the linear domain. Parallelepiped-shaped specimens were machined along the flow direction from disks, with the following dimensions $5 \times 2 \times 1 \text{ mm}^3$. Heating rate was $1^\circ\text{C}/\text{min}$.

The α transition temperature, T_α , was defined as the temperature at which the tangent of the loss angle, $\tan \delta = E''/E'$, was maximum. This temperature is depicted on figure 2 for the 5 PETs as a function of frequency. The temperature of α transition at 1 Hz is often used as a characteristic of amorphous polymer, it is given in table 2. The five materials exhibit different T_α and different

crystallization temperatures (visible with the increase in modulus on Figure 1 above 110 °C). Modulus at rubbery plateau also differs from one PET to another. In parallel, T_g , the glass transition temperature, were estimated using DSC (Differential Scanning Calorimetry) for heating rate of 10 °C/min. T_g are also given in Table2. From those data one can conclude that working temperature could range between 85 to 120 °C for all materials.

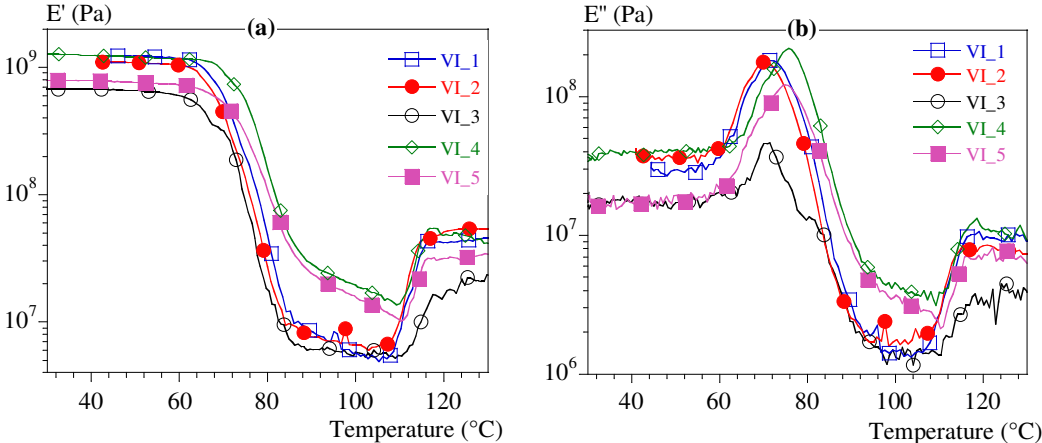


Figure 1: Evolution of conservative, E' , (a) and loss modulus, E'' , (b) with temperature during DMA analysis. Mode is sinusoidal tension-tension with a strain amplitude of $3 \cdot 10^{-3}$. Heating rate is 1 K/min. Comparison of the five PET resins.

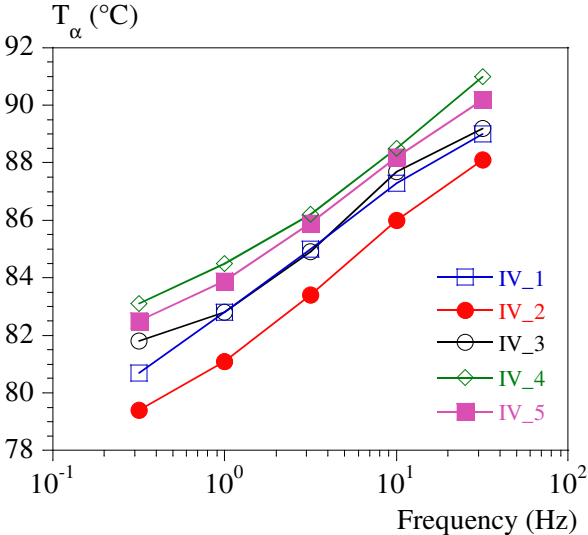


Figure 2: α transition temperature (T_α) vs. frequency deduced from DMA analysis in sinusoidal tension-tension mode with a strain amplitude of $3 \cdot 10^{-3}$. Heating rate is 1 K/min. Comparison of the five PET resins.

To go deeper in the characterization of the material, isothermal frequency sweeps (from 0.1 to 100 Hz), performed every five degrees between 75 and 100 °C, allowed classical WLF approach [5, 29-31] that combines frequency and temperature effects. Master curves, at an arbitrary reference temperature,

T_{ref} , of 90 °C, were built (figure 3 a). Shift factors, $a_{T/T_{ref}}$, that only depend on temperature, T, could be represented using Williams, Landel and Ferry (WLF) approach [5, 29] with a correlation of 98 % (eq. (1):

$$a_{T/T_{ref}} = 10^{-\frac{c_1(T-T_{ref})}{c_2+T-T_{ref}}} \quad (1)$$

where C_1 and C_2 are scalar parameters depending on material and on T_{ref} .

When reference temperature is taken at T_g , C_1 and C_2 becomes C_1^g and C_2^g , respectively. The difference between T_g and C_2^g is sometimes considered as the minimal temperature for α process to be efficient at infinite time, T_∞ . Data are given in table 2. Only the VI_2 resin, which is a little branched, exhibited values of C_i^g that were out of the usual range.

The master curves at 90 °C were used in previous study [1]. The choice of T_g as reference temperature allowed to account for differences in T_g in the analyses and results in a slightly reduced scattering of different curves. This has been already suggested to compare materials in an easier manner when T_g are significantly different (e.g., PET and PEF [16]). Figure 3 depicts the master curves and the shift factors at T_g . These latter exhibit a pretty good correlation with T_∞ , for their part.

Ref.	Reference temperature of 90 °C		Tg as reference temperature		Tg (°C)	T_α (°C)	T_∞ (°C)
	C_1	C_2	C_1^g	C_2^g			
VI_1	10	61	12.2	50	79	82.8	29
VI_2	2.1	26	4.3	13	77	81.1	64
VI_3	6.7	45	8.6	35	80	82.8	45
VI_4	10	56	11.9	47	81	84.5	34
VI_5	7.7	45	9.7	36	81	83.9	45

Table 2: Data resulting of WLF analysis of DMA traces at 1Hz in tension.

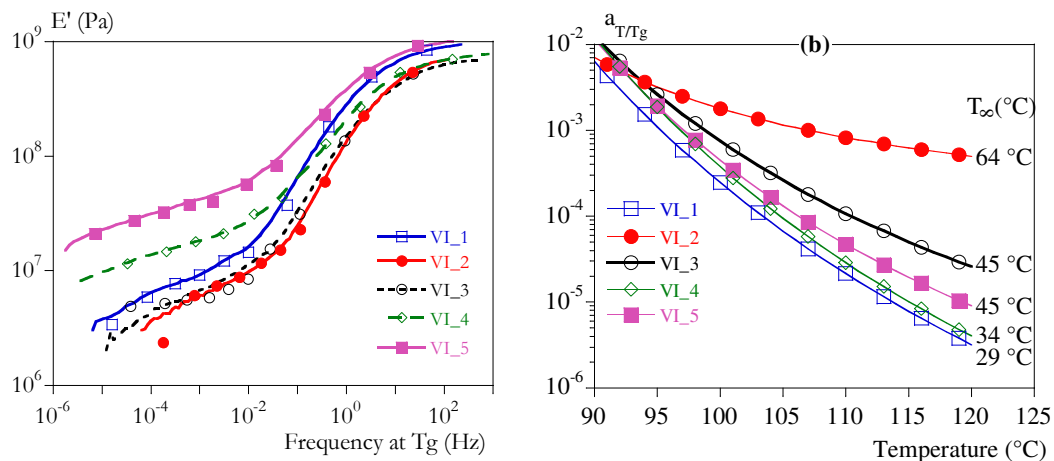


Figure 3: Master curves (a) and shift factors (b) at Tg. Coefficients are gathered in table 2.

The large strain behavior was investigated according to protocols built up in previous studies [9-16]. Flat hourglass-shaped specimens with a thickness of 2 mm were tooled from injection molded disks. Local true strain was measured thanks to a seven dots video extensometer as suggested by G'ssell et al. [33]. Incompressibility was assumed as usually. Instron 1341 universal machine with an ambiance chamber were used. Tests were performed at temperatures of 80, 85 and 95 °C. Crosshead velocities were kept constant during tension and was of 0.5, 10 or 150 mm/s. This corresponded to targeted equivalent strain rates at 90°C ranging from 0.005 to 100 s⁻¹, which is the processing range (see below). Table 3 allows comparing those equivalent strain rates to technological data for better understanding.

Results are depicted in terms of longitudinal local extension (or draw ratio), λ , or Hencky's strain, $\epsilon = \ln(\lambda)$. They are referred to with equivalent strain rate at Tg $\dot{\epsilon}_{T_g}$ (Figure 4).

As describes in the literature [17, 22, 23, 33-35] the deformation of all PETs at temperatures close to their glass transition temperatures appears to be constrained by the elasticity of a rubber-like network. Typical "stress vs. strain" tensile curves are depicted in Figure 4a for two equivalent strain rates (10⁻⁴ and 10⁻² s⁻¹ at Tg) for VI_3 and VI_5. One can observe that behavior of the different materials is equivalent once compared in the same physical state (e.g., same $\dot{\epsilon}_{T_g}$). A drastic strain hardening exists that allowed to define their natural draw ratios (NDR) at the onset of strain hardening [1]. This NDR is the key parameter that defines the maximal potential extension upon loading. It depends on temperature and strain rate, being lower at high strain rate or low temperature. Nevertheless, stress at NDR (figure 4b) only depends on equivalent strain rate at Tg, whatever the PET is. Strain at NDR, for its part depends on materials when strain rate at Tg is lower than 0.01 s⁻¹.

Ref.	0.005 s ⁻¹ at 90 °C				100 s ⁻¹ at 90 °C			
	$\dot{\epsilon}_{T_g}$ (s ⁻¹)	at 80°C (s ⁻¹)	at 85°C (s ⁻¹)	at 95°C (s ⁻¹)	$\dot{\epsilon}_{T_g}$ (s ⁻¹)	at 80°C (s ⁻¹)	at 85°C (s ⁻¹)	at 95°C (s ⁻¹)
VI_1	3.1 10 ⁻⁵	5.5 10 ⁻⁵	6.3 10 ⁻⁴	0.03	0.6	1.1	12.8	572
VI_2	3.5 10 ⁻⁵	2.2 10 ⁻⁴	1.5 10 ⁻³	0.01	0.7	4.5	30.8	222
VI_3	6.1 10 ⁻⁵	6.1 10 ⁻⁵	7.3 10 ⁻⁴	0.02	1.2	1.2	14.6	466
VI_4	6.1 10 ⁻⁵	3.4 10 ⁻⁵	5.2 10 ⁻⁴	0.03	1.2	0.7	10.5	658
VI_5	5.7 10 ⁻⁵	3.0 10 ⁻⁵	5.3 10 ⁻⁴	0.03	1.1	0.6	10.7	597

Table 3: Equivalence of strain rates in s⁻¹. Comparison of strain rates at testing temperatures (80, 85 and 95 °C) with equivalent strain rates at 90 °C and at Tg ($\dot{\epsilon}_{T_g}$).

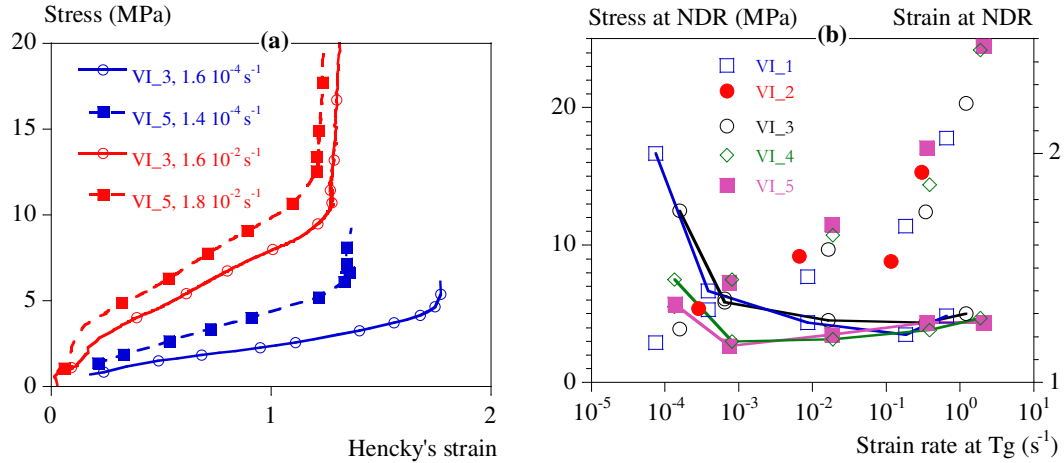


Figure 4: Behavior of PET upon uni axial tension. a) Comparison between two materials (VI_3 and VI_5) for two strain rates at Tg (10^{-4} s^{-1} in blue and 10^{-2} s^{-1} in red). b) Stress (symbols) and strain (symbols and lines) at NDR (Natural Draw Ratio) for all PETs vs. strain rate at Tg. See Table 2 and 3 for correspondence with technical values.

To conclude, the chosen materials are of the same type but can differ by their chain mobilities, their α transition temperatures, their rigidities, their sensitiveness to temperature and their NDRs (Table 2 and figures 3 & 4). Unfortunately, no simple correlation could be found at this stage between chains characteristics and those data.

However, the set of materials allows exploring a wide range of possible behaviors for PETs. Rubbery modulus as well as the gap in modulus at α transition vary by a factor of 10, Tg vary by several degrees and strain at NDR also depends on temperature and strain rate. The use of equivalent strain rate at Tg allowed to combine strain rate and temperature effects, so that one can compare behavior of PETs in an equivalent physical state. Experimental loading conditions must be adjusted to each of them when it is desired to load them in the same state, i.e., promoting the same type of behavior and elementary processes.

3. Biaxial kinematics through blowing of preforms

Despite of the fact that the prototype makes it possible to reproduce industrial heating that promotes thermal gradient within the thickness of the preform and thermal profile along its length, heating was ruled for the temperature to be as uniform as possible, in and along the preform. IR heating did not allow, nevertheless, precisely controlling temperature. Obviously, it would have been possible to heat the preform using an ambiance chamber. However, this would have led to much longer heating time (as heating throughout the thickness would had relied on conduction) and it should endanger the tests due to possible cold crystallization for temperature higher than $100 \text{ }^\circ\text{C}$.

In consequence tests could not be compared at the same temperature but only at temperature “close enough”. Conversely, no static crystallization could occur so that materials remained amorphous before stretching. Additionally, for clarity only results without pre-stretching will be reported here.

So, following part focus on the description of free blowing (without mold) of isothermal preforms. The shape of the preform is given on figure 5. Grids (5x5 mm) were tooled on the surface that allowed to measure local longitudinal, λ_1 , and transversal, λ_2 , draw ratios (resp. strain). An IR pyrometer allowed to address the temperature of the preform during blowing and estimating the relative importance of self-heating. Results that are reported below concerns the top part of the body of the preform (2 cm from bottom of the neck).

Test were performed at temperatures ranging from 89 °C to 118 °C, which corresponded to temperatures deduced from figure 1. Maximum pressure was 0.5 MPa but, similarly to industrial devices, only air flux was imposed (but not measured) and was constant upon the entire study.

Final volume ranged from around 600 mL to almost 2000 mL depending on material and temperature. The huge change in volume during blowing resulted in a strong coupling with pressure. In consequence, pressure was measured as a function of time inside the preform. Blowing duration was 200 ms, which is conform to industrial uses.

Typical blowing kinematics are illustrated in figure 5 from high-speed video sequences. Overall, the steps did not depend on materials neither on temperatures. However, kinetics highly varies from one material to another and from a temperature to another. It can be concluded that, despite the relative low differences between the nature of the resins, their respective processing ranges can be significantly different. The sharpness of pressure peak is a convenient trace for kinetics: the sharper the peak the more rapid the blowing, the lower the pressure the easier the blowing.

The testing protocol is such that loading initially consists of a ramp of pressure inside the preform. A constant slope of 17.4 MPa/s was observed whatever the temperature, or the material were (Figure 6). Afterwards, the slope of the curve “pressure vs. time” first decreased and finally a drastic drop in pressure occurred. This was already reported in the past and corresponds to classical coupling between the volume of the blown part and the pressure for the given air flux [2]. The pressure at which the change in slope occurred corresponded to the beginning of inflation (Figure 5). It depended on the material and on the temperature (Figure 7). At that moment, volume increased too rapidly compared to air flux. However, there is no simple correlation between elastic modulus on figure 1 or 3a and this pressure suggesting a not elastic behavior. In example, the lowest pressure was observed for VI_1, which did not exhibit the lowest elastic modulus. PET VI_3 and VI_2, which are very similar in terms of moduli, had different behavior upon blowing.

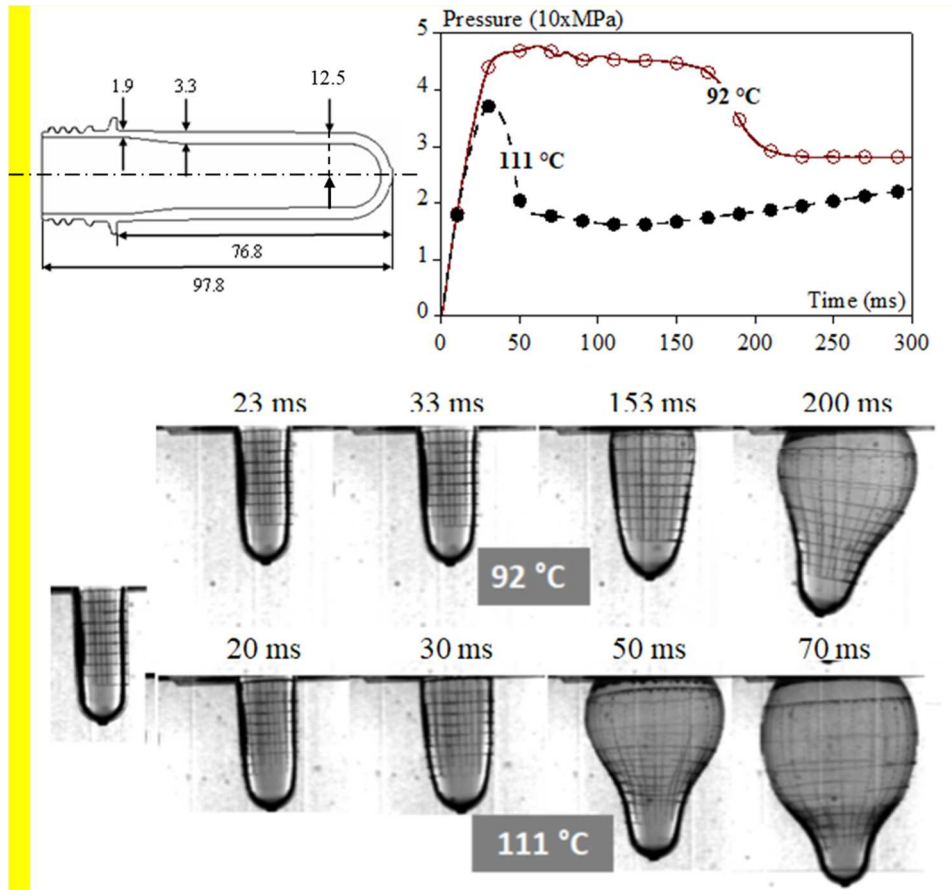


Figure 5: Typical sequences for blowing; Comparison between VI_3 at 92 °C and 111 °C. Top left: Shape and dimension of preforms (in mm). Top right: pressure vs. time curves. Bottom photographs at different steps of blowing (times are materialized on photographs).

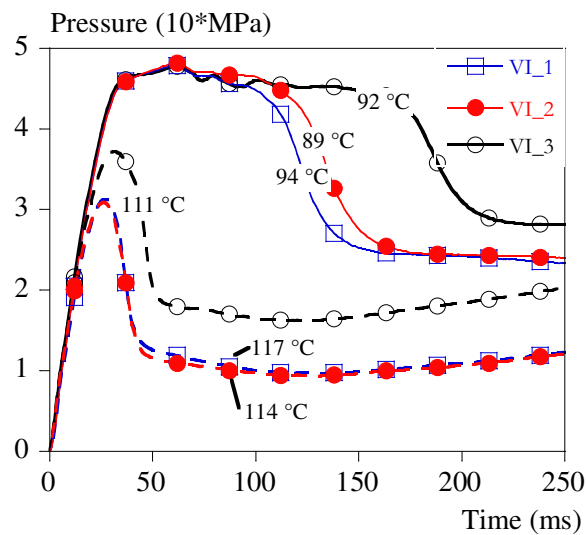


Figure 6: Pressure vs. time for blowing. Comparison between VI_1, 2 and 3 at temperatures close to 90 °C and close to 115 °C: (□) VI_1, 94 °C and 117 °C; (●) VI_2, 89 °C and 114 °C; (○) VI_3, 92 °C and 111 °C.

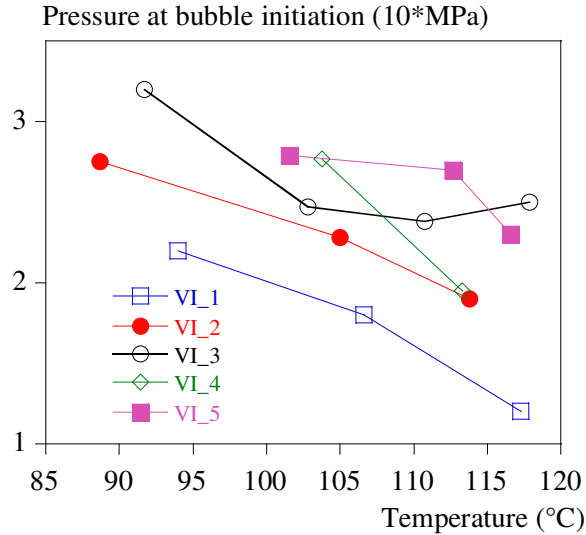


Figure 7: Pressure at inflation vs. temperature for 5 PETs of the study: (□) VI_1; (●) VI_2; (○) VI_3; (◇) VI_4; (■) VI_5.

For a better understanding, Figure 8 superimposes the evolutions of pressure, longitudinal and transversal draw ratios, and longitudinal and transversal strain rates (for PET VI_3 at four temperatures, as an example). The very first step of deformation was always close to a planar orthoradial tension ($\lambda_2 > 0$ while $\lambda_1 = 0$ in Figure 8) which turned to simultaneous, but not equilibrated, bi axial tension when inflation is noticeable. This initiation of biaxiality was nevertheless, earlier at higher temperature (Figures 8d) and depended on the PET. Supplementary figure 1 depicts this latter aspect by plotting the ratio λ_2/λ_1 as a function of time for two PETs. Indeed, λ_2 is significantly higher than λ_1 in the first stage. VI_1, which was the easiest to blow PET, reached a volume ranging from 1000 mL to 1900 mL for temperatures ranging from 90 °C to 117 °C [1]. It also exhibited a quasi-equiaxial deformation at the end of blowing. Conversely, VI_5 exhibited the smallest volume (634 mL to 876 mL [1]) with a clearly higher transversal strain. Looking at details this bi-axiality also depended on temperature. Once NDR was reached a rapid increase in temperature could be recorded (by 10 °C, supplementary figure 2) but initiation and propagation of the deformation remained isothermal, hence we could analyze them.

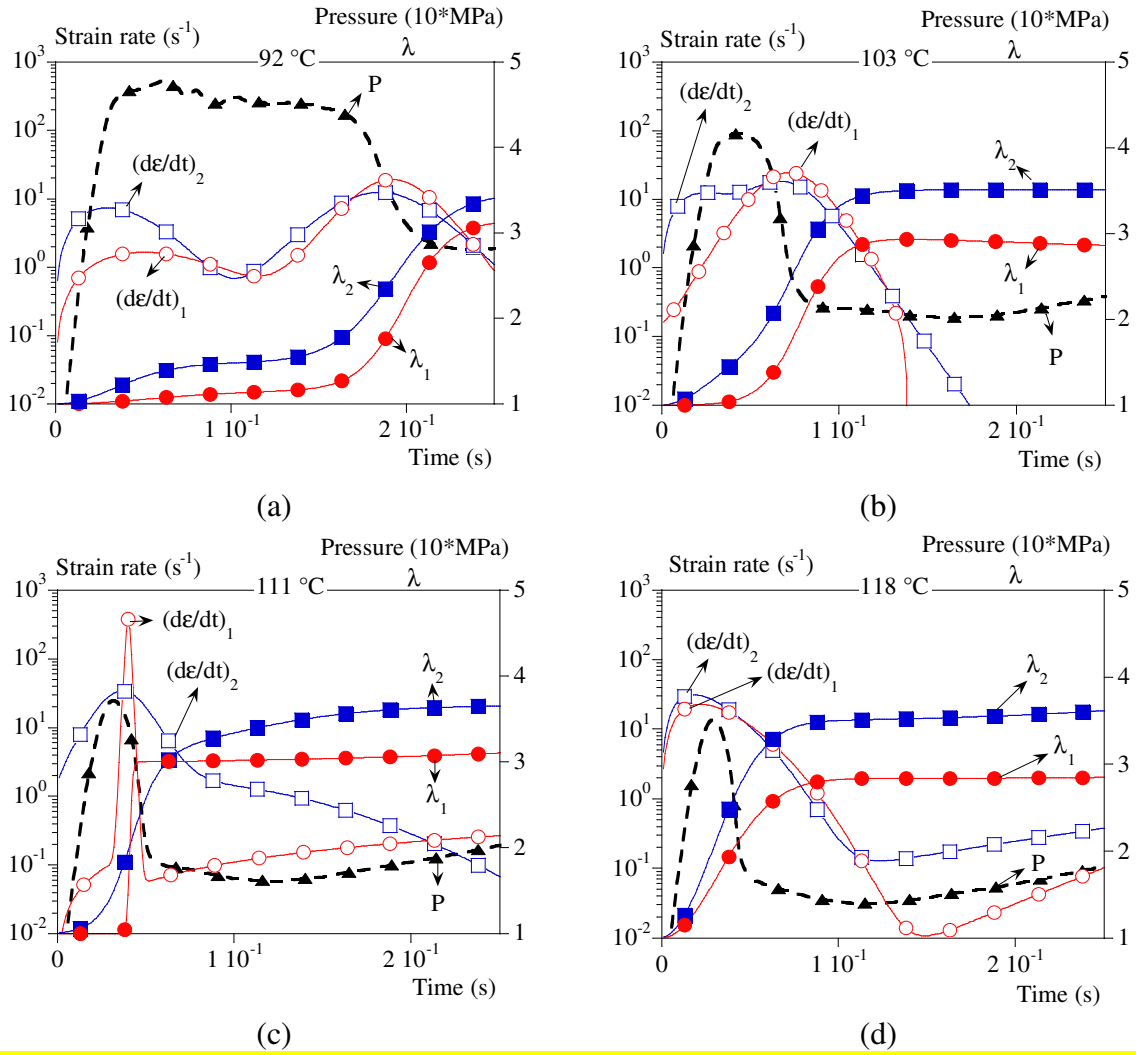


Figure 8: Blowing sequences for VI_3. Comparison of four temperatures: 92 (a), 103 (b), 111 (c) and 118 °C (d). Evolution upon time of pressure (P, ▲), longitudinal strain rate ($\left(\frac{d\varepsilon}{dt}\right)_1$, ○), transversal strain rate ($\left(\frac{d\varepsilon}{dt}\right)_2$, □), longitudinal draw ratio (λ_1 , ●), transversal draw ratio (λ_2 , ■).

Accounting for the minimum thickness, e (1.9 mm), and the average diameter, D (24.9 mm), the order of magnitude for stress at inflation, σ , could be estimated at 1 to 2 MPa ($\sigma = \text{Pressure times } D/2e$). Inflation stress could then be compared to uniaxial tensile stress of figure 4a. This confirmed that blowing is initiated when material exhibit its rubber like behavior.

During the linear increase in pressure strain rate increased in a similar manner whatever the materials or the temperatures were (figure 9). After inflation began the strain rate rapidly reached an almost constant in time value (if temperature is high enough, i.e., higher than 90 °C in present conditions). Maximal strain rate depended on temperature and on material. Order of magnitude was a few to a few tens of s^{-1} for the two components of tensor we considered (longitudinal or transversal) (Figure 9 a and b). The existence of a limited value for strain rate is one of the manifestations of visco elasticity and hardening behavior observed in figure 4a. As strain increases, thickness decreases,

which would result in an acceleration, but stress increases due to hardening and an increase in strain rate would also result in an additional hardening.

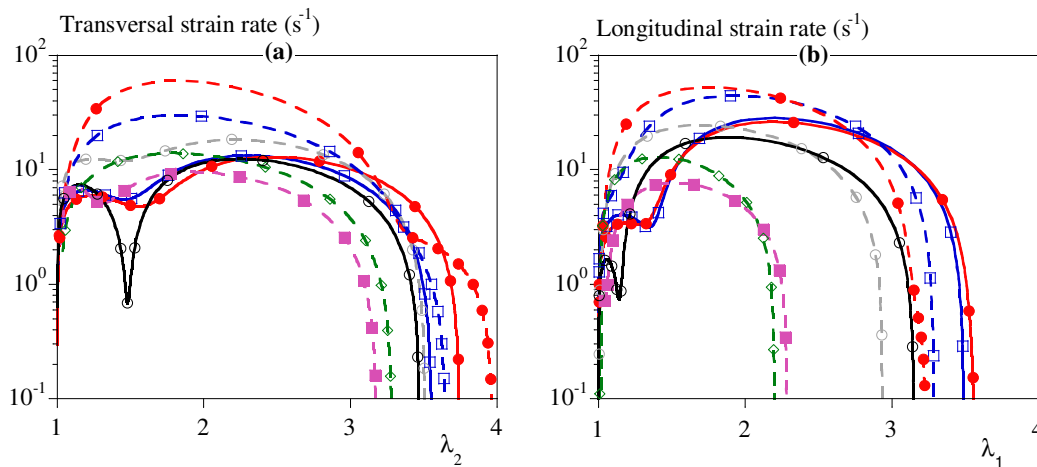


Figure 9: Transversal (a) and longitudinal (b) strain rates vs. respective draw ratios λ_2 and λ_1 ; Comparison between temperatures close to 90 °C (symbols and plain lines) and temperatures close to 100 °C (symbols and dashed lines) for different PETs: (□) VI_1, 94 °C and 107 °C; (●) VI_2, 89 °C and 105 °C; (○) VI_3, 92 °C and 103 °C; (◇) VI_4, 104 °C; (■) VI_5, 101 °C.

4. Discussion

4.1 Kinematics

To conclude the above description, schematic of deformation could be the following:

1. Air flux and initial volume of preform controls a rate of pressure increase. Then material experience a short period of transverse planar tension. Initial rigidity of PET and pressure rate rule the strain rate in the material.
2. Strain rate and temperature rules the behavior of PET and in particular apparent yield stress.
3. Once pressure is equal to that yield stress necking is initiated, which results in inflation of a bubble. The lower the temperature or the higher the pressure rate, the higher the inflation pressure.
4. The stretching can take then place being easier and easier as thickness decreases. In parallel material strain hardens (figure 4a) and any increase in strain rate makes it more rigid. Combining all these events strain rate is then stabilized. The higher the temperature the higher the strain rate.
5. Once NDR is reached deformation stops, and strain rate rapidly tends to zero.

4.2 Stretching range

In consequence, as it should be expected stiffness of the material at test temperature is a key parameter that controls blowing of PETs. However, when looking at their respective master curves at Tg VI_3 and VI_2 seem to be very similar. VI_4 exhibits an intermediate modulus whereas VI_5 is the more rigid of our set. Pressure at inflation is not totally correlated with this ranking. This suggests that another parameter should be accounted for to rank blow ability. The intuitive data should be strain rate.

The equivalent strain rate at Tg showed all its interest at this level. Figure 10 gathers and compares maximum strain rates and equivalent strain rates at Tg in the transversal and in the longitudinal directions. Strain rate at the temperatures of the tests ranged between 0.8 to 60 s⁻¹. Equivalent strain rate at Tg ranged from 0.1 to 10⁻⁴ s⁻¹, which corresponds strictly to rubbery plateau of figure 3 and confirms that PET is loaded in its rubbery state. According to figure 4b it is also a domain where strain hardening of PETs can be different. Consequently, some resins (e.g., VI_4 and 5) could exhibit a low strain at NDR that could makes it more difficult to blow the largest bottles or at the lowest temperatures. This could result in some aspect defaults (pearly aspect) and should be later accounted for. Finally, it is also worth noticing here that the equivalent strain rate decreases for increasing temperature.

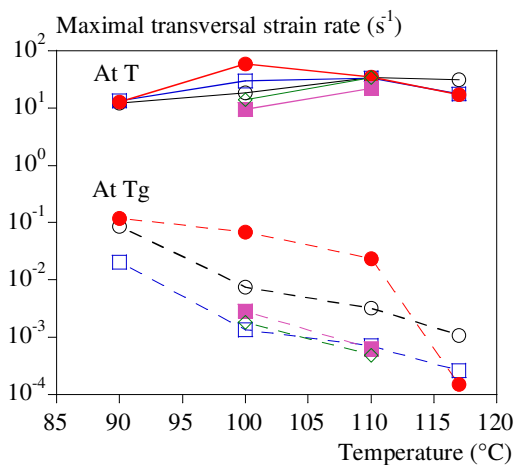


Figure 10: Maximal transversal strain rate observed in the study vs. temperature of the test; Comparison between actual strain rate and strain rate at Tg for VI_1 (□); VI_2 (●); VI_3 (○); VI_4 (◇); VI_5 (■).

4.3 Usefulness of time temperature superposition principle

From above results one could assess stretchability using equivalent strain rate at Tg but shift factors at Tg, a_{T/T_g} , should also be accounted for. This is illustrated in the following. For better

reading, our further analyze of **stretchability**, thanks to time temperature superposition principle, was based on thickness reduction. According to eq. (2), assuming the polymers to be incompressible:

$$\lambda_3 = \frac{1}{\lambda_1 \lambda_2} = \frac{e}{e_0} \quad (2)$$

where e and e_0 are the thickness at time t and the initial thickness, respectively.

The points we wish to demonstrate below are the facts that:

- Equivalent strain rates at a reference temperature are convenient parameters to be used (as it was demonstrated in tension and shearing [9-14, 36]) even for describing blowing conditions.
- Differences between resins could have been anticipated from master curves and parameters a_{T/T_g} .

To achieve that point, general frame is first illustrated comparing resins 3 and 2 and then applied to understand stretching ranges of resins 2, 4 and 5 compared to that of resin 3 (medium range PET according to supplier, Tergal Fibre).

4.3.1 VI_2 vs. VI_3

In the set of material, VI_3 and VI_2 led to similar master curves at T_g (Figure 3a). Despite of this these two PETs cannot be stretched in totally equivalent conditions (Figure 11a). At low temperature (close to $90\text{ }^\circ\text{C}$) both VI_3 and VI_2 can be blown but are demanding of a long time, i.e., potentially longer than 0.2 s which is the usual blowing time. The consequence would be, in an industrial context, that natural draw ratio (NDR), which limits lowering of thickness, may not be reached. Additionally, strain induced crystallization might not be induced before the end of the forming. VI_2 stretching is faster at $89\text{ }^\circ\text{C}$ than that of VI_3 at $92\text{ }^\circ\text{C}$. Increasing temperature makes blowing faster in the two cases, so that NDRs are reached during blowing.

On figure 11a one could conclude that time of blowing is comparable for those two polymers between $103\text{ }^\circ\text{C}$ and $118\text{ }^\circ\text{C}$. However, strong difference exists that is **visible** on figure 11b comparing draw ratios vs. time for VI_2 at $105\text{ }^\circ\text{C}$ and for VI_3 at $103\text{ }^\circ\text{C}$. Initiation of transversal deformation is delayed for VI_2 compared to VI_3 despite of a higher temperature. Conversely, the longitudinal deformation occurs sooner. Therefore, loading of VI_2 is significantly closer to a simultaneous bi-axial loading and its overall kinetics of blowing is more rapid despite of a later initiation. Same conclusion could be drawn from blowing at $114\text{ }^\circ\text{C}$ for VI_2 and $111\text{ }^\circ\text{C}$ for VI_3.

Figure 12 depicts the elastic modulus of VI_2 and VI_3 as a function of equivalent strain rate at T_g . **An average strain rate of 10 s^{-1} was assumed according to our measurements** (Figure 9 and 10). Stiffness of VI_3 is slightly higher than that of VI_2. Shift factors are also reported as a function of temperature. From blowing temperature one can deduce shift factor for the two PETs. This latter

parameter is significantly higher for VI_2 above 100 °C and exhibit a much lower dependence with the temperature.

Equivalent strain rate at T_g, $\dot{\epsilon}_{T_g}$, can then be calculated for all the conditions of figure 11. They are materialized with lines for VI_3 and with cross and squares for VI_2. During the blowing (10 s⁻¹) the elastic modulus of VI_2 at 92 °C is higher than the elastic modulus of VI_2 at 89 °C, according to that analysis. Hence, that is the reason why the blowing of VI_2 was more rapid. At these temperature shift factors are equivalent for the two materials. So, stiffness is the only parameter to account for to anticipate differences in kinematics.

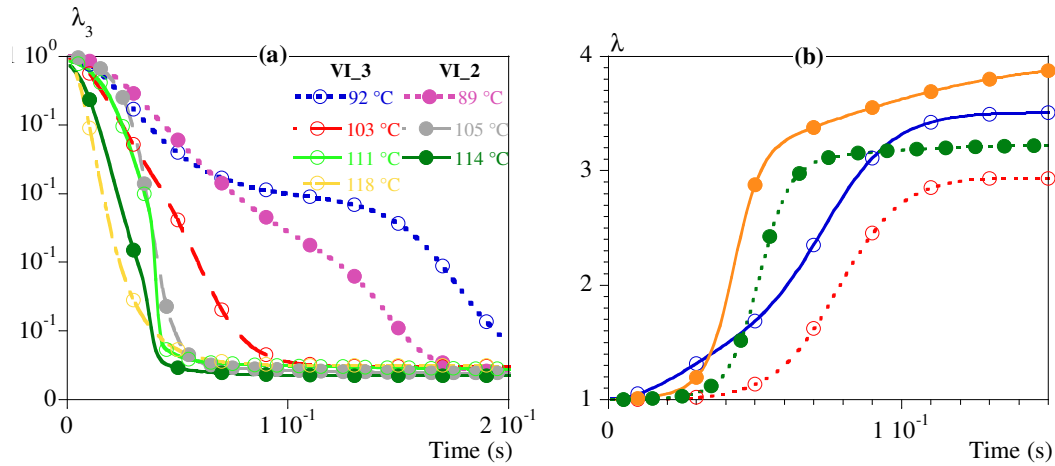


Figure 11: In the thickness draw ratio vs. time during blowing of VI_3 and VI_2. a) Comparison between λ_3 at different temperatures (see legend) for VI_3 (○) and VI_2 (●). b) Blowing kinetics: comparison of longitudinal (λ_1 , dotted lines), transversal (λ_2 , plain lines) of VI_3 (○ and ○) at 103 °C and VI_2 (● and ●) at 105 °C vs. time.

Above 100 °C, the differences in stiffness explain that initiation of blowing was a little postponed for VI_2 at 105 °C and 114 °C compared to VI_3 at 103 ° (Figure 11a before time 0.05 s). The differences in shift factor explain that:

- Firstly, increasing the temperature is much less efficient to rule behavior for VI_2 compared to VI_3. Indeed, modulus of VI_2 is only reduced by 5.5 % between 105 °C and 114 °C when loaded at 10 s⁻¹, whereas the decrease is 24 % for VI_3 between 103 °C and 111 °C for the same strain rate.
- Secondly, the initial transversal uniaxial stage is constrained and reduced in duration for VI_2. In fact, due to high values for a_{T/T_g} , increase in strain rate, due to thinning upon loading, results in a bigger increase of the strain rate at T_g (resp., of the modulus). Consequently, hardening due to strain rate lowers the transversal strain rate up to the moment when longitudinal deformation can take place.

If one would have wished to blow VI_2 similarly to VI_3, varying the pressure could have helped in counterbalancing the difficulty to rule behavior through temperature. Additionally, stretching prior to blowing could have helped ruling biaxiality.

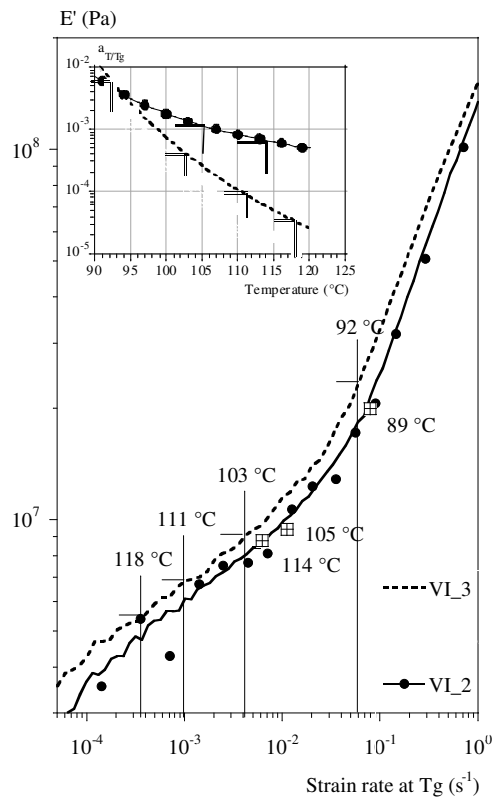


Figure 12: Analysis of stretch abilities of VI_2 (●) and VI_3 (dashed lines) in terms of equivalent strain rate at Tg for the same actual strain rate of 10 s⁻¹. Main curve: E' vs. equivalent strain rate at Tg; lines represent conditions for VI_3 in figure 11; Cross and squares represent conditions for VI_2 in figure 11; Temperatures are respective temperature of tests. Medallion depicts shift factor vs. temperature; Lines correspond to temperature of the tests.

4.3.2 Stretchability compared to that resin VI_3

Stretchability of any polymers cannot be seen as a general and intrinsic property. A target must be first defined in terms of conditions and maximum draw ratio. Stretchability of any the polymers cannot be seen as a general and intrinsic property. A target must be first defined in terms of conditions and maximum draw ratio. In the following we will assume that kinetics for blowing of any our resins should be close to the kinematics observed on resin VI_3 at 103 °C (Figure 8b). This could be due to the necessity of keeping of the properties of bottles unchanged when passing from one resin to another.

From the online measurements (Figure 8b and eq. (2)), it was observed that the “trough thickness” strain rate $\left(\frac{d\varepsilon}{dt}\right)_3$, supplementary figure 3) ranged from 5 s⁻¹ to 42 s⁻¹. According to Figure 3b, the

value for a_{T/T_g} at 103 °C for VI_3 was $3.887 \cdot 10^{-4}$. In consequence, nominal blowing of VI_3 corresponded to an equivalent strain rate at T_g ranging between $1.9 \cdot 10^{-3}$ to $1.6 \cdot 10^{-2} \text{ s}^{-1}$ upon time.

Assuming that stiffness of the resins is the first parameter to be accounted for to assess feasibility of blowing, it can be concluded that nominal blowing is possible (for the given conditions of pressure and of design of preform) **when elastic modulus ranges from $7.46 \cdot 10^6 \text{ Pa}$ to $1.28 \cdot 10^7 \text{ Pa}$.**

From Figure 3a, the equivalent strain rates that allowed each of the resin to exhibit such range of moduli could be estimated (cf. supplementary figure 4 for graphical illustration). **Then, Figure 3b made it possible to evaluate values of a_{T/T_g} that would lead to actual strain rates of 5 s^{-1} for the higher modulus and 42 s^{-1} when modulus if the lowest, respectively.** In isothermal conditions two temperatures were deduced from those latter values: T_{\min} , which represents the minimal temperature to reach for the material to exhibit an initial modulus such that a 5 s^{-1} deformation is possible; T_{\max} , which represents that maximal temperature to reach for the material to exhibit a final modulus such that a 42 s^{-1} deformation would occur. T_{\min} is the limit of stretch ability, below that temperature blowing **could be too slow**. Above T_{\max} material could be not stiff enough to limit strain rates à 42 s^{-1} . Table 4 gathers those data. This analysis is confronted to some of our **observations** in Figures 13 to 16.

	$\dot{\epsilon}_{T_g} \text{ (s}^{-1}\text{)}$		$a_{T/T_g} \text{ (-)}$		$T_{\min} \text{ (}^\circ\text{C)}$	$T_{\max} \text{ (}^\circ\text{C)}$
	for 5 s^{-1}	for 42 s^{-1}	for 5 s^{-1}	for 42 s^{-1}	for 5 s^{-1}	for 42 s^{-1}
PET						
VI_1	$3.9 \cdot 10^{-3}$	$2.7 \cdot 10^{-4}$	$7.80 \cdot 10^{-4}$	$6.43 \cdot 10^{-6}$	96	116
VI_2	$2.6 \cdot 10^{-2}$	$3.0 \cdot 10^{-3}$	$5.16 \cdot 10^{-3}$	$7.12 \cdot 10^{-5}$	92	>140
VI_4	$5.9 \cdot 10^{-5}$	$2.9 \cdot 10^{-6}$	$1.18 \cdot 10^{-5}$	$6.90 \cdot 10^{-8}$	114	125
VI_5	Not accessible below 120 °C					

Table 4: Equivalent strain rates, $\dot{\epsilon}_{T_g} \text{ (s}^{-1}\text{)}$, shift factors, $a_{T/T_g} \text{ (-)}$, and temperatures that allow stretching resins from 5 s^{-1} to 42 s^{-1} .

Figure 13 superimposes draw ratios, λ_1 , λ_2 and λ_3 , for VI_1 as a function of time compared to targeted result (VI_3 at 103 °C). When temperature is lower than T_{\min} ($94 \text{ }^\circ\text{C}$ compared to limit of $96 \text{ }^\circ\text{C}$) the stretching is significantly slower. When temperature is in between T_{\min} and T_{\max} ($107 \text{ }^\circ\text{C}$) the blowing time and blowing kinetics are close to that of VI_3 at 103 °C, whereas if temperature is higher than upper limit ($117 \text{ }^\circ\text{C}$ instead of $116 \text{ }^\circ\text{C}$ in table 4) the blowing schematics changes.

Figure 14 superimposes same types of results concerning VI_2. In the same manner the above procedure allowed to anticipate the lower temperature to be reached. Concerning upper limit our previous analysis pointed out that increasing temperature would have had a limited effect due to the evolution of shift factor upon temperature. It would have been dangerous to test PET above $120 \text{ }^\circ\text{C}$

due to crystallization. Nevertheless, Figure 14 confirms that increasing temperature above 105 °C (e.g., to 114 °) would not be a good solution and that this PET (as suggested above) **gains being blown** at lower temperature than VI_3.

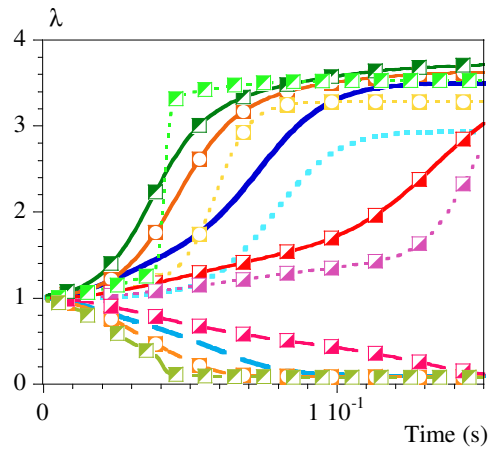


Figure 13: Comparison of draw ratios for VI_1 (symbols) to the targeted blowing of VI_3 at 103 °C (Thick lines blue). Dark plain lines are λ_2 , light colored dotted lines are λ_1 and light-colored dashed lines are λ_3 . Results for three temperatures are superimposed for VI_1: 94 °C (mauve, red, pink, and green), 107 °C (orange and yellow) and 117 °C (green).

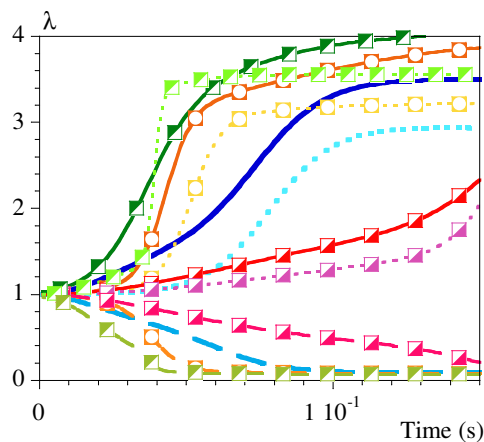


Figure 14: Comparison of draw ratios for VI_2 (symbols) to the targeted blowing of VI_3 at 103 °C (Thick lines blue). Dark plain lines are λ_2 , light colored dotted lines are λ_1 and light-colored dashed lines are λ_3 . Results for three temperatures are superimposed for VI_1: 89 °C (mauve, red, pink, and green), 105 °C (orange and yellow) and 114 °C (green).

Figure 15 deals with VI_4 for which it is possible to reproduce blowing of VI_3 at 103 °C by **heating it at 116 °C**. In that case, 104 °C is too low for blowing the preform. Finally, it was not possible to stretch VI_5 even at 117 °C (Figure 16).

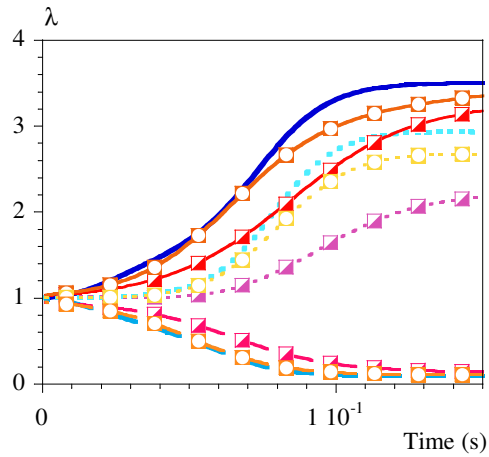


Figure 15: Comparison of draw ratios for VI_4 (symbols) to the targeted blowing of VI_3 at 103 °C (Thick lines blue). Dark plain lines are λ_2 , light colored dotted lines are λ_1 and light-colored dashed lines are λ_3 . Results for two temperatures are superimposed for VI_1: 104 °C (▣, red, pink, and mauve) and 116 °C (◻, orange and yellow).

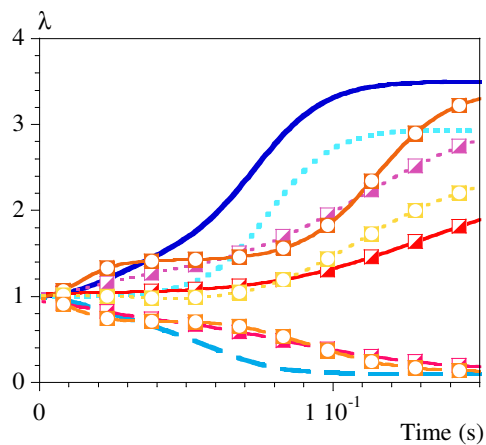


Figure 16: Comparison of draw ratios for VI_5 (symbols) to the targeted blowing of VI_3 at 103 °C (Thick lines blue). Dark plain lines are λ_2 , light colored dotted lines are λ_1 and light-colored dashed lines are λ_3 . Results for two temperatures are superimposed for VI_1: 101 °C (▣, red, pink and mauve) and 117 °C (◻, orange and yellow).

4.3.3 Summary

To summarize, if the “a posteriori” analyze (Figure 3) we described were have been done prior to blowing, it would have been possible to anticipate that, to blow resins 1,2, 4 and 5 in an equivalent manner than VI_3 at 103 °C using the same air flux:

- VI_1 could must be heated up between 96 °C and 116 °C. In parallel, its higher sensitiveness to temperature (cf. shift factors) could tend to make increase in temperature more efficient to lower down its stiffness.
- the control of modules of VI_2 from temperature could be difficult, as its sensitiveness to temperature is much lower than that of VI_3. It should thus be blown at temperature lower than 103 °C, possibly adjusting pressure.
- VI_4 should be heated up to 114 °C and, as for VI_1, its sensitiveness to the temperature is high, so that blowing close to the lower limit could be the best solution.

This should be refined but represents a proof of feasibility.

5. Conclusion

In this study, biaxial behavior of PET was addressed using a free blow prototype representative for Injection Stretch Blow Molding. Though some equivalent attempts exist in the literature [4], such study, that intend fundamentally to characterize PET within the range of stretching processes, is still unusual.

Tests were applied to well characterized resins that exhibited significantly different behaviors to illustrate the range of stretchability, and of glass transition temperatures, that could be faced during recycling.

The results confirmed, as already suggested [1, 15, 16, 22, 23, 37], that strain rate is always such as the material remains on its rubbery plateau whatever the material is. In addition, as demonstrated for simple tests [9-14, 36], time temperature superposition principle can be taken at profit to characterize testing conditions with one unique parameter: the equivalent strain rate at reference temperature. To our knowledge, formal proof in the context of processing, as that developed here, are still rare in the literature.

Choice was made to use T_g as reference temperature, which allowed to compare materials in same "physical states". Stresses that are developed at inflation are of same order of magnitude of those measured during uniaxial test for similar equivalent strain rate at reference temperature [1]. This justifies and simplifies the extrapolation of laboratory tests to forming conditions, which is often done blindly so far.

Moreover, the spirit for a route to assess for stretchability of different resins from the analysis of master curves and from shift factor a_{T/T_g} is suggested. At this stage, knowing the performance of one resin, which one wishes to reproduce with a new resin, it is possible to anticipate a range of temperature within which the second and unknown resin should be heated up to exhibit similar behavior upon blowing.

This protocol should be improved to gain in predictability and to be usable in the context of real ISBM. Further studies should then extend the analysis to more complex loadings (i.e., stretch blowing) and to blends of resins or even to recycled PET to be complete.

Nevertheless, one can hope that, in the future, this kind of approach will help in the recycling of PET by leading to a simple protocol, based on simple laboratory analysis, to face variability of recycled resins.

As it stands, this first step is obviously encouraging, and the protocol will already be an effective aid to study the evolution of the stretchability of PET during recycling cycles more efficiently as it simplifies the choice of test conditions and gives a route for extrapolation from laboratory conditions to process.

References

1. Deloye E, Haudin JM, Billon N, *Int. Polym. Proc.*, **3**: 358-369 (2012)
2. Tan CW, Menary GH, Salmeia Y, Armstrong CG, Picard M et al., *Int. J. Mater. Form. Suppl*, **1**: 799-802 (2008)
3. Billon N, Haudin JM, Vallot C, Babin C, *Int. Polym. Proc.*, **30** :487-499 (2015)
4. Nixon J, Menary GH., Yan S, *Int. J. of Material Forming*, **10**:765–777 (2017)
5. Ferry JD, "Viscoelastic properties of polymers" John Wiley & Sons (1980)
6. Arruda M, Boyce MC, Jayachandran R, *Mechanics of Materials*, **19(2)**:193–212 (1995)
7. Buckley CP, Jones DC, Jones DP, *Polymer*, **37(12)**:2403–2414 (1996)
8. Nasraoui M, Forquin P, Siad L, Rusinek A, *Materials & Design*, **37**:500–509 (2012)
9. Billon N, *J Appl Polym Sci*, **125**:4390-4401 (2012)
10. Federico CE, Bouvard JL, Combeaud C, Billon N, *Polymer*, **139**:177 – 187 (2018)
11. Federico CE, Bouvard JL, Combeaud C, Billon N, *Polymer*, **202**:122710 (2020)
12. Gehring F, Bouvard JL, Billon N, *J Appl Polym Sci*, **133(35)**:43837-43853 (2016)
13. Maurel-Pantel A, Baquet E, Bikard J, Bouvard JL, Billon N, *Int J Plast*, **67**:102-126 (2015)
14. Fabre V, Quandalle G, Billon N, Cantournet S, *Polymer*, **137**: 22-29 (2018).
15. Billon N, Picard M, Gorlier E, *Int. J. of Mater. Forming*, **7(3)**: 1–10 (2014)
16. Forestier E, Combeaud C, Guigo N, Sbirrazzuoli N, Billon N, *Polymer*, **203**:122755 (2020)
17. Long SD, Ward IM, *J. Appl. Polym. Sci*, **42**, 1921-1929 (1991)
18. Lorentz G, Tassin JF, *Polymer*, **35(15)** :3200-3205 (1994)

19. Al Itry R, Lamnawar K, Maazouz A, Billon N, Combeaud C, *European Polym. J.*, **68**: 288-301 (2015)
20. Sweeney J, Ward IM, *Polymer*, **36**, (2), 299-308 (1995)
21. Matthews RG, Duckett RA, Ward IM, Jones DP, *Polymer*, **38(19)**: -4802 (1997)
22. Gorlier E, Agassant JF, Haudin JM, Billon N, *Plastics, Rubber and Composites*, **30(2)**: 48-55 (2001)
23. Gorlier E, Haudin JM, Billon N, *Polymer*, **42(23)**: 9541-9549 (2001)
24. Le Bourvellec G, Monnerie L, Jarry JP, *Polymer*, **27**: 856-860 (1986)
25. Lapersonne P, Tassin JF, Monnerie L, Beautemps J, *Polymer*, **32, (18)**: 3331-3339 (1991)
26. Salem DR, *Polymer*, **33(15)**:3182-3188 (1992)
27. Faisant de Champchesnel JB, Bower DI, Ward IM, Tassin JF, Lorentz G, *Polymer*, **34(18)**: 3763-3770 (1993)
28. Vigny M, Tassin JF, Gibaud A, Lorentz G, *Polym. Eng. Sci.*, **37(11)**: 1785-1794 (1997)
29. WILLIAMS ML, LANDEL RF, FERRY JD, *J. American Chem. Soc.*, **77**: 3701-3707 (1955)
30. Shaw MT, MacKnight WJ, *Introduction to polymer*, Wiley & Sons (2005).
31. Ward IM, Sweeney J, *Mechanical properties of solid polymers*, John Wiley & Sons (2012)
32. G'sell C et al., *Int. J. Solids Struct.*, **39**:3857-3872 (2002)
33. Le Bourvellec G, Beautemps J, Jarry JP, *J. Appl. Polym. Sci*, **39**:319-328 (1990)
34. Gordon DH, Duckett RA, Ward IM, *Polymer*, **35(12)**: 2554-2559 (1994)
35. Ward IM, *Polym. Eng. Sci.*, **24(10)**: 724-736 (1984)
36. Diani J, Gilormini P, Arrieta JS, *Polymer*, **58**:107-112 (2015)
37. Menager C, Guigo N, Martino L, Sbirrazzuoli N, Visser H, et al., *Polymer*, **158**:364-371 (2018)

